



HAL
open science

FracVAL: An improved tunable algorithm of cluster–cluster aggregation for generation of fractal structures formed by polydisperse primary particles

José Carlos Moran Cofré, A. Fuentes, Franklin Liu, Jérôme Yon

► To cite this version:

José Carlos Moran Cofré, A. Fuentes, Franklin Liu, Jérôme Yon. FracVAL: An improved tunable algorithm of cluster–cluster aggregation for generation of fractal structures formed by polydisperse primary particles. *Computer Physics Communications*, 2019, 239, pp.225-237. 10.1016/j.cpc.2019.01.015 . hal-02094957

HAL Id: hal-02094957

<https://hal.science/hal-02094957>

Submitted on 22 Oct 2021

HAL is a multi-disciplinary open access archive for the deposit and dissemination of scientific research documents, whether they are published or not. The documents may come from teaching and research institutions in France or abroad, or from public or private research centers.

L'archive ouverte pluridisciplinaire **HAL**, est destinée au dépôt et à la diffusion de documents scientifiques de niveau recherche, publiés ou non, émanant des établissements d'enseignement et de recherche français ou étrangers, des laboratoires publics ou privés.



Distributed under a Creative Commons Attribution - NonCommercial 4.0 International License

FracVAL: An Improved Tunable Algorithm of Cluster-Cluster Aggregation for Generation of Fractal Structures Formed by Polydisperse Primary Particles

J. Morán^{a,c,*}, A. Fuentes^a, F. Liu^b, J. Yon^c

^a*Departamento de Industrias, Universidad Técnica Federico Santa María, Av. España 1680, Casilla 110-V, Valparaíso, Chile*

^b*Measurement Science and Standards, National Research Council of Canada, Ottawa, Ontario, Canada*

^c*Normandie Univ, INSA Rouen, UNIROUEN, CNRS, CORIA, 76000 Rouen, France.*

Abstract

In this study, the tunable algorithm of cluster-cluster aggregation developed by Filippov et al. 2000 for generating fractal aggregates formed by monodisperse spherical primary particles^{R1.C5} is extended to polydisperse primary particles. This new algorithm, termed FracVAL^{R1.C5}, is developed by using an innovative aggregation strategy^{R1.C0}. The algorithm is able to preserve the prescribed fractal dimension $(D_f)^{R1.C4}$ and prefactor $(k_f)^{R1.C4}$ for each aggregate, regardless of its size, with negligible error for lognormally distributed primary particles with the geometric standard deviation $\sigma_{p,geo}$ being as large as 3. In contrast, for polydisperse primary particles the direct use of Filippov et al. 2000 method, as is done by Skorupski et al. 2014, does not ensure the preservation of D_f and k_f for individual aggregates and it is necessary to generate a large number of aggregates to achieve the prescribed D_f and k_f on an ensemble basis. The performance of FracVAL is evaluated for aggregates consisting of 500 and 1000^{R2.C4} monomers and for fractal dimension variation over the entire range of D_f between 1 and 3 and k_f between 0.1 and 2.7^{R1.C5}. Aggregates consisting of 500 monomers^{R2.C4} are generated on average in less than 2.4 minutes on a common laptop, illustrating the efficiency of the proposed algorithm.

*Corresponding author.
E-mail address: morancoj@coria.fr

Keywords: Tunable Algorithm; Fractal Aggregates; Polydisperse Primary Particles; Cluster-Cluster Aggregation

Program Summary

Program Title: FracVAL

Catalogue identifier:

Program summary URL:

Program obtainable from:

Licensing provisions: GNU General Public License

No. of lines in distributed program, including test data, etc.: 2,120

No. of bytes in distributed program, including test data, etc.: 139,264

Distribution format: ZIP

Programming language: Fortran 90

Computer: PC

Operating system: Windows and Linux

RAM: 1.0 Gb

Classification:

Nature of problem:

Generation of fractal-like aggregates, consisting of point-touching, polydisperse primary particles

Solution method:

Hierarchical cluster-cluster random aggregation

Additional comments including Restrictions and Unusual features:

Possible combinations of fractal dimension and prefactor depend on monomers polydispersity

Running time: Depends on the number of monomers and fractal parameters for each polydispersity level

1. Introduction

Fractal-like aggregates formed by nearly spherical primary particles are frequently encountered in many applications, such as in colloidal or aerosol systems, combustion systems, and flame synthesis of functional nanoparticles. Such particles have some remarkable and unique characteristics, e.g. large surface area and porous geometry, implying that they have high absorption capacity, good catalyst performance, fast dissolution, light-weight, and require relatively little solid material to occupy large space [1]. These particles are generated by aggregation processes which can be theoretically classified into two categories, particle-cluster [2, 3, 4, 5, 6] (PC) and cluster-cluster (CC) aggregation. A complete review of different algorithms focused on these aggregation mechanisms is found in [7]. Additionally, optimized^{R1.C5} version of these algorithms can be found in more recent studies [8, 9, 10].

Under the idea of fixing the fractal dimension, Thouy and Jullien [11] introduced the first tunable CC aggregation algorithm. Subsequently, several studies are conducted to propose different tunable algorithms for fractal aggregate generation [12, 13, 14, 15, 16], though most of these studies preserved only the fractal dimension. One remarkable exception is the algorithm developed by Filippov et al. [13], which is able to preserve both the fractal dimension and the prefactor, paving the way to investigate the individual effect of D_f and k_f on the morphology and physical properties of fractal aggregates [17, 18, 19]. Some distinct features of tunable algorithms can be highlighted: (1) they allow systematic studies of the individual effects of either D_f or k_f on the physical properties of fractal aggregates; (2) a large number of aggregates can be generated numerically with a considerably low computational time; and (3) they allow the generation of fractal aggregates with prescribed D_f and k_f over a wide range irrespective of the physical aggregation mechanism.

Almost all the existing tunable algorithms developed in the literature rely on the assumption of monodisperse primary particles. One exception is the code developed by Skorupski et al. [20], which is based on the method of Filippov et al.^{R1.C5} [13] and can be used to generate fractal aggregates formed by polydisperse spherical primary particles. However, the direct application of the Filippov et al.^{R1.C5} [13] algorithm to generate fractal aggregates formed by polydisperse primary particles, as conducted by Skorupski et al. [20], encounters the difficulty that the resultant individual aggregates do not preserve the prescribed fractal dimension. It is important to overcome this issue

38 and to develop a tunable algorithm to efficiently generate fractal aggregates
 39 formed by polydisperse primary particles, which can then be used to fill some
 40 existing gaps with regard to the effect of primary particle polydispersity on
 41 morphological properties, such as the center of mass, inertia moment, radius
 42 of gyration of sub-clusters being aggregated and consequently on the result-
 43 ing structures [21, 22], as well as various physical and optical properties.

44 Since practical colloid or aerosol aggregates consist of polydisperse pri-
 45 mary particles, various studies have been conducted in order to assess its
 46 influence on their morphological characterization [23, 24, 25, 21, 22], and
 47 the physical or chemical properties of such particles, such as kinetics of co-
 48 agulation and sintering or coalescence, light scattering, mobility and set-
 49 tling [26, 27, 28, 29, 30, 31, 32, 33, 22, 34, 35]. In 2012 Eggersdorfer and
 50 Pratsinis [21] found **found a dependency between aggregates morphology and**
 51 **monomers polydispersity.**^{R1.C0} Based on the above **mentioned studies**^{R1.C0}, it
 52 is important to develop efficient tunable algorithms to generate fractal ag-
 53 gregates formed by polydisperse PP with known D_f and k_f .

54 In this study, an improved hierarchical tunable algorithm of CC aggrega-
 55 tion is developed based on the algorithm of Filippov et al. [13] to generate
 56 numerically fractal aggregates formed by polydisperse PPs.

57 2. Theoretical background

58 2.1. Primary particle size distribution

59 The nearly spherical primary particles constituting fractal aggregates,
 60 such as soot, fumed silica and titania, encountered in practice are always
 61 polydisperse and the primary particle size distribution (PPSD) can be com-
 62 monly described by either the normal or lognormal probability density func-
 63 tions [36, 37]. Nevertheless, the normal distribution is not practical because
 64 for large standard deviations of the distribution it can lead to negative PP
 65 radii. Eq. (1) presents the lognormal probability density function of PP radii,

$$f[r_p] = \frac{N}{\ln[\sigma_{p,geo}] \sqrt{2\pi} r_p} \exp \left[-\frac{1}{2} \left(\frac{\ln[r_p] - \ln[r_{p,geo}]}{\ln[\sigma_{p,geo}]} \right)^2 \right], \quad (1)$$

66 where $f[r_p]dr_p$ is the probability of finding a particle with a radius between r_p
 67 and $r_p + dr_p$, $r_{p,geo}$ and $\sigma_{p,geo}$ correspond to the geometric mean and geometric
 68 standard deviation, respectively. **Please note that for a population of N**
 69 **monomers these values are given by the following equations,**^{R2.C1}

$$\log(r_{p,geo}) = \frac{\sum_{i=1}^N \log(r_i)}{N} \quad (2a)$$

$$\log(\sigma_{p,geo}) = \sqrt{\frac{\sum_{i=1}^N (\log(r_i) - \log(r_{p,geo}))^2}{N}} \quad (2b)$$

70
71 It can be checked that for monodisperse primary particles the RHS of
72 Eq. (2b) becomes zero and therefore $\sigma_{p,geo} = 1$.^{R2.C1} Although the level of
73 PP polydispersity is often fairly low with $\sigma_{p,geo} \leq 1.3$, highly polydisperse
74 primary particles can be encountered. For example, for flame generated
75 soot aggregates, the geometric standard deviation $\sigma_{p,geo}$ can be as high as
76 $\sigma_{p,geo} = 2.1$ [36, 37, 38, 39], depending on the residence time, fuel type, and
77 flame conditions.

78 2.2. Characterization of fractal aggregates

79 The mass of a fractal aggregate (m_a) follows the fractal scaling law. For
80 an aggregate consisting of point-touch polydisperse spherical PPs [21],

$$\frac{m_a}{\overline{m}_p} = k_f \left(\frac{R_g}{r_{p,geo}} \right)^{D_f}, \quad (3)$$

81 where \overline{m}_p is the average PP mass, i.e., $m_a/\overline{m}_p = N$, is the number of PP
82 in the aggregate. The exponent D_f and the proportionality constant k_f
83 in Eq. (3) are the fractal dimension and prefactor, respectively. For frac-
84 tal aggregates consisting of monodisperse monomers ($\sigma_{p,geo} = 1$) generated
85 through diffusion-limited cluster aggregation (DLCA), it has been well es-
86 tablished that $D_f \approx 1.78$ and $k_f \approx 1.40$ [7, 40]. However, Eggersdorfer and
87 Pratsinis [21] showed a dependency of both D_f and k_f on PP polydispersity.
88 In fact, for aggregates formed in the same molecular regime they found that
89 both D_f and k_f decrease with increasing PP polydispersity. They obtained
90 $D_f = 1.68$ and $k_f = 0.98$ for $\sigma_{p,geo} = 2.0$, and $D_f = 1.48$ and $k_f = 0.77$ for
91 $\sigma_{p,geo} = 3.0$. The ranges of these parameters are used for the generation and
92 analysis of fractal aggregates of the present work. Finally, R_g is the radius of
93 gyration of the aggregate calculated using the expression proposed by [22],

$$R_g^2 = \frac{1}{m_a} \sum_{i=1}^N m_{p,i} [(R_i - R_c)^2 + r_{g,i}^2], \quad (4)$$

94 where $r_{p,i}$ and $m_{p,i}$ are respectively the PP radius and mass of the i th spher-
 95 ical primary particle, which is located at a distance R_i from the origin of a
 96 fixed coordinate system. The term $r_{g,i}$ is the radius of gyration of the i th
 97 PP, i.e., $r_{g,i}^2 = (3/5)r_{p,i}^2$. R_c is the center of mass of the aggregate evaluated
 98 as,

$$R_c = \frac{1}{m_a} \sum_{i=1}^N m_{p,i} R_i. \quad (5)$$

99 It can be easily shown that Eqs. (4) and (5) degrade to those for monodisperse
 100 primary particles given in Filippov et al. [13] when all the primary particles
 101 have the same mass.

102 3. Formulation of the improved tunable algorithm

103 3.1. Main equations

104 Consider two clusters (aggregates) with mass m_1 and m_2 and radius of
 105 gyration R_{g1} and R_{g2} , which have the same prescribed D_f and k_f and are to
 106 be aggregated to form a larger aggregate with mass $m = m_1 + m_2$ and radius
 107 of gyration R_g and to preserve both D_f and k_f . To this end, it can be shown
 108 that the distance between the mass centers of the two clusters Γ satisfies the
 109 following equation,

$$m^2 R_g^2 = m (m_1 R_{g1}^2 + m_2 R_{g2}^2) + \Gamma^2 m_1 m_2, \quad (6)$$

110 The consequence and advantage of using Eq. (6), as it will be demonstrated
 111 later, are that it ensures the preservation of both D_f and k_f ^{R1.C5} during each
 112 step of the aggregation process for each individual aggregate generated. The
 113 derivation of this equation is provided in Appendix A. In the special case of
 114 two aggregates consisting of N_1 and N_2 monodisperse PPs ($N = N_1 + N_2$),
 115 Eq. (6) is reduced to,

$$N^2 R_g^2 = N (N_1 R_{g1}^2 + N_2 R_{g2}^2) + \Gamma^2 N_1 N_2, \quad (7)$$

116 which is identical to the relationship derived by Filippov et al. [13], i.e., the
 117 derived Eq. (6) is the generalized form of Eq. (7) for aggregates consisting of
 118 polydisperse PPs. Eq. (6) represents an original contribution of the present
 119 study and forms one of the main relations of the present tunable algorithm.

120 *3.2. FracVAL: A tunable cluster-cluster aggregation algorithm*

121 The FracVAL (fractal aggregate generation algorithm developed in Val-
 122 paraíso) algorithm is programmed in a hierarchical manner, i.e., only ag-
 123 gregation between sub-clusters with approximately the same number of pri-
 124 mary particles is allowed [11]. The algorithm consists of four main steps
 125 corresponding to the flow chart shown in Fig. 6 and it is described as follows.

126 **Step 1:** The fractal dimension D_f (between 1 and 3) and the fractal pref-
 127 actor k_f (a positive value, typically on the order of unity) of aggregates to
 128 be generated are prescribed, which will be preserved during the entire fractal
 129 aggregate generation process. In addition, the primary particle radius distri-
 130 bution and the aggregate size N (the number of primary particles contained
 131 in the aggregate) are also required. The PPSD is assumed lognormal and
 132 characterized by the geometric mean and standard standard deviation, i.e.,
 133 $r_{p,geo}$ and $\sigma_{p,geo}$. To obtain a total of N radii from this lognormal distribu-
 134 tion given by Eq. (1), a pseudo-random number generator is used [41]. To
 135 avoid extremely large and extremely small values of PP radius, which are
 136 unrealistic, the selection of PP radii is constrained to the following range
 137 $[r_{p,geo}/\sigma_{p,geo}^2, r_{p,geo}\sigma_{p,geo}^2]$, which contains 95.5% of the radii.

138 **Step 2:** A particle-cluster aggregation algorithm is first used to obtain a
 139 total of I_t sub-clusters (smaller aggregates) consisting of approximately the
 140 same number of primary particles (N_{sub}), where $\sum_{I_t} N_{sub} = N$. This criterion
 141 is introduced in order to mimic the hierarchical aggregation of particles that
 142 possess the self-similarity of fractal aggregates [42]. In the present work N_{sub}
 143 is selected depending on N . For $N \in [50, 500]$, each **sub-cluster^{R1.C5}** consists of
 144 $N_{sub} = 0.1N$ and under the lower limit ($N \leq 50$) a constant $N_{sub} = 5$
 145 is employed. On the other hand, above the upper limit ($N \geq 500$) a constant
 146 $N_{sub} = 50$ **is^{R1.C5} used**. **This type of particle-cluster aggregation algorithms**
 147 **has been found to experience some difficulties for retaining exactly the fractal**
 148 **parameters and therefore small N_{sub} are recommended in the literature in**
 149 **order to avoid effects in the final aggregates [13, 20]. In this context, a**
 150 **sensitivity analysis is included in the Appendix C. The main conclusion of**
 151 **this analysis is that for $N_{sub} < 0.15N$ there is not effect on the morphology**
 152 **of final aggregates. Additionally, an variation of $\pm 20\%$ of D_f or k_f for the**
 153 **initial sub-clusters is expected to have a relatively small effect on the density-**
 154 **density correlation function of the final aggregates.^{R1.C4}**

155 **Step 3:** In this step, the sub-clusters generated in Step 2 are organized
 156 into pairs that are able to aggregate to form a larger cluster. This “ability to
 157 aggregate” is defined according to the criterion $R_{max,1} + R_{max,2} \geq \Gamma_{12}$, where

158 $R_{max,i}$ corresponds to the furthest distance of a PP to the center of mass of
 159 the i th aggregate ($i = 1,2$) and Γ_{12} is the distance between the centers of
 160 mass of the two sub-clusters to be aggregated and calculated as,

$$\Gamma_{12} = \frac{1}{\sqrt{m_1 m_2}} [m^2 R_g^2 - m (m_1 R_{g1}^2 + m_2 R_{g2}^2)]^{1/2}, \quad (8)$$

161 where m_1 , m_2 , R_{g1} and R_{g2} are the masses and radii of gyration of the two
 162 sub-clusters being aggregated. Additionally, $m = m_1 + m_2$ and R_g are the
 163 corresponding parameters for the resulting larger aggregate. The radii of
 164 gyration R_{g1} , R_{g2} and R_g are calculated from the scaling law,

$$R_{gi} = r_{p,geo} \left(\frac{n_i}{k_f} \right)^{1/D_f} \quad (9)$$

165 where n_i is the number of monomers of the i th aggregate (here for both
 166 the sub-clusters and the resultant larger aggregate) and D_f and k_f are the
 167 prescribed fractal parameters.

168 **Step 4:** This is the main part of the algorithm. In this step, the two
 169 sub-clusters belonging to the same pair determined in Step 3 are aggregated
 170 to form a larger aggregate. It is based on the idea that there are two sub-
 171 clusters, from here onwards they will be called sub-cluster A1 (containing
 172 N_1 monomers) and sub-cluster A2 (containing N_2 monomers), that can be
 173 aggregated in many different ways, each of these ways associates a distance
 174 between the center of mass of aggregates A1 and A2, but there is only one
 175 distance (represented by Γ_{12} in Eq. (8)) that ensures the preservation of
 176 both D_f and k_f . Therefore, knowing this distance, our goal only consists
 177 in finding one of the possible paths to combine the clusters by keeping the
 178 distance between them fixed.^{R2.C3} To better describe this step, it is divided
 179 into 6 sub-steps as shown in Fig. 6.

- 180 • **Sub-step a:** Select a pair of sub-clusters A1 and A2^{R2.C3} from the
 181 pairs determined in Step 3.
- 182 • **Sub-step b:** Create a binary matrix a_{ij} . Let d_{i1} and d_{j2} be respectively
 183 the distance from the center of monomer i (in A1, $i = 1,2,\dots,N_1$) and j
 184 (in A2, $j = 1, 2,\dots, N_2$) to the center of mass of A1 and A2, respectively.
 185 Assign $a_{ij} = 1$ when:

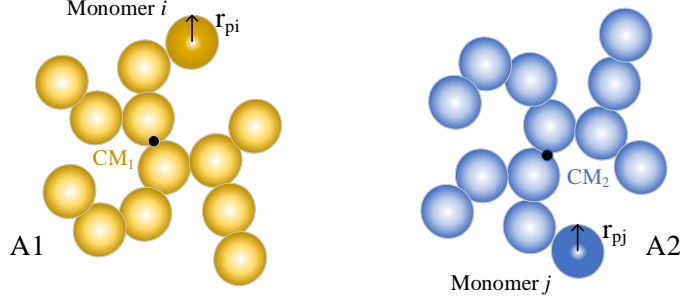


Figure 1: Sub-clusters A1 and A2 selected to be aggregated.

186 The restriction defined by Eq. (10) is fulfilled, this restriction ensures
 187 that both monomers are close enough to be in point-touching,

$$D_{i1,+} + D_{j2,+} \geq \Gamma_{12}, \quad (10)$$

188 where $D_{i1,+} = d_{i1} + r_{pi}$, $D_{i1,-} = d_{i1} - r_{pi}$, $D_{j2,+} = d_{j2} + r_{pj}$ and
 189 $D_{j2,-} = d_{j2} - r_{pj}$. Additionally, there is a lower limit defined by 3
 190 possible cases described as follows,

- 191 – Case 1: When the spheres of radius $D_{i1,+}$ and $D_{j2,+}$ can be inter-
 192 sected (see Fig. 2), this means that $|D_{i1,+} - D_{j2,+}| \leq \Gamma_{12}$.
 193 The two following cases are associated with the intersection of the
 194 spheres with radius $D_{i1,-}$ and $D_{j2,-}$.
- 195 – Case 2: When the sphere of radius $D_{i1,+}$ is too big containing
 196 the sphere of radius $D_{j2,+}$, i.e. when $(D_{i1,+} - D_{j2,+}) > \Gamma_{12}$ with
 197 an^{R1.C5} upper limit $D_{i1,-} \leq \Gamma_{12} + D_{j2,+}$.
- 198 – Case 3: Analogously, when the sphere of radius $D_{j2,+}$ is too big
 199 containing the sphere of radius $D_{i1,+}$, i.e. when $(D_{j2,+} - D_{i1,+}) >$
 200 Γ_{12} with an upper limit $D_{j2,-} \leq \Gamma_{12} + D_{i1,+}$.

201 Please note that Case 2 and Case 3 are theoretically and mathemat-
 202 ically possible, and they are considered in FracVAL. Please see the
 203 Appendix D for a further explanation of Cases 2 and 3.^{R1.C1} However,

204 Case 1 is considered the most common one, and therefore it is used to
 205 explain the subsequent steps of the algorithm.

206 These restrictions ensure that i th monomer belonging to A1 is able to
 207 aggregate with the j th monomer belonging to A2; otherwise, assign
 $a_{ij} = 0$. For the pair A1 and A2, Γ_{12} is evaluated using Eq. (8).

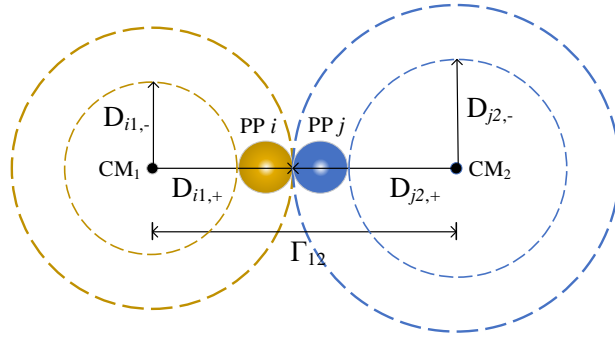


Figure 2: Example of intersection between the spheres of radius $D_{i1,+}$ and $D_{j2,+}$ can be intersected.

208

- 209 • **Sub-step c:** Loop over the elements of the binary matrix a_{ij} . If $a_{ij} = 0$,
 210 continue the loop. If $a_{ij} = 1$, assign the i th primary particle in A1 as
 211 s1 and the the j th primary particle in A2 as s2.

212

213 The goal of Step 4 is to aggregate the sub-clusters A1 and A2. Specif-
 214 ically, the algorithm needs to find the locations of the mass centers of
 215 A1 and A2 and the proper orientations of A1 and A2 upon aggregation
 216 to satisfy the following restrictions:

217 First, the distance between the centers of mass of A1 and A2 is Γ_{12} given
 218 by^{R1.C5} Eq. (8). Secondly, the selected primary particle candidates s1
 219 (belonging to A1) and s2 (belonging to A2) are in point-touch. Thirdly,
 220 there is no overlapping between any primary particles in A1 and A2.
 221 The above mentioned 3 restriction will be satisfied progressively by 3
 222 stages described as follows,^{R1.C2}

- 223 – **Stage 1:** To satisfy restriction 1 we retain the center of mass of A1
 224 (referenced as $CM1 = (X_{cm,1}, Y_{cm,1}, Z_{cm,1})$) fixed while the center

225
226
227

of mass of A2 (referenced as $CM2 = (X_{cm,2}, Y_{cm,2}, Z_{cm,2})$) is placed at a distance Γ_{12} from $CM1$. This displacement is made along the unitary direction defined by $CM1$ and the center of $s1$. At this point we already fulfil restriction 1. This is shown in Fig. 3.^{R1.C2}

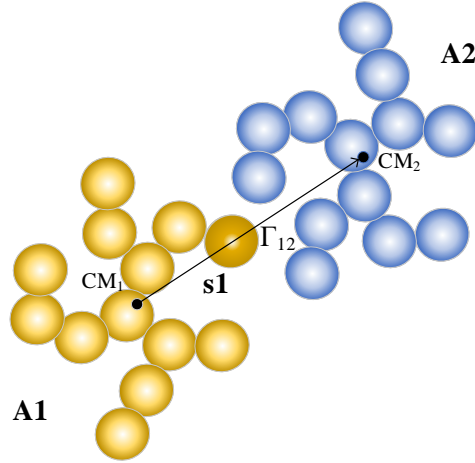


Figure 3: Displacement of A2 to fulfill restriction (1).

228
229
230
231
232
233
234

- **Stage 2:** Next, we will rotate A1 and A2 in the following manner to fulfill restrictions 2 and 3. Firstly, A1 is rotated, to this end we calculate the distances d_{s1} and d_{s2} from monomers $s1$ and $s2$ to $CM1$ and $CM2$, respectively, and place the monomer $s1$ at a tangential point defined by the interception of two of the following spheres as illustrated in Fig. 4.^{R1.C2}

$$D_{s1,+}^2 = (X - X_{cm,1})^2 + (Y - Y_{cm,1})^2 + (Z - Z_{cm,1})^2, \quad (11a)$$

235

$$D_{s2,+}^2 = (X - X_{cm,2})^2 + (Y - Y_{cm,2})^2 + (Z - Z_{cm,2})^2, \quad (11b)$$

236
237
238

This random point can be determined analytically by considering the following procedure (Here the reader may go directly to Stage 3 without loss of continuity). As shown in Fig. 5, the sphere-sphere

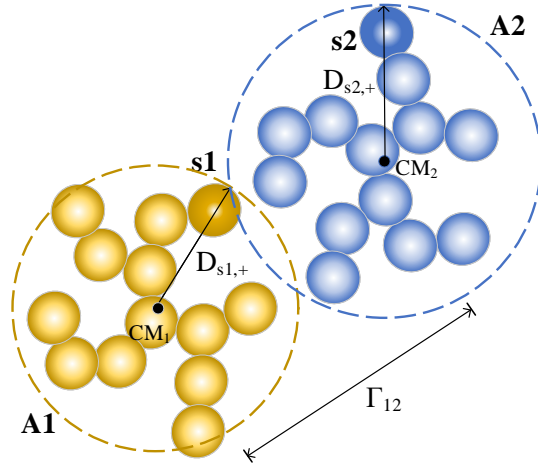


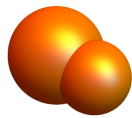
Figure 4: Location of monomer s_1 given by the intersection of spheres given by Eq. (11a) and Eq. (11b).

239
240

intersection corresponds to a circle that can be parametrized by the equation (12),^{R1.C2}

$$\vec{r}[\psi] = \vec{c} + \rho \cos[\psi] \hat{i}' + \rho \sin[\psi] \hat{j}', \quad \psi \in [0, 2\pi] \quad (12)$$

(a) Sphere-sphere intersection



(b) Parametrized circle

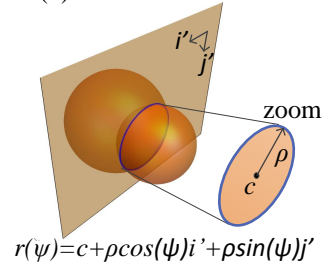


Figure 5: Sphere-sphere intersection and circle parametrization.

241
242

where \vec{c} and ρ are the coordinates of the geometric center and the radius of this circle, respectively. Additionally, \hat{i}' and \hat{j}' are

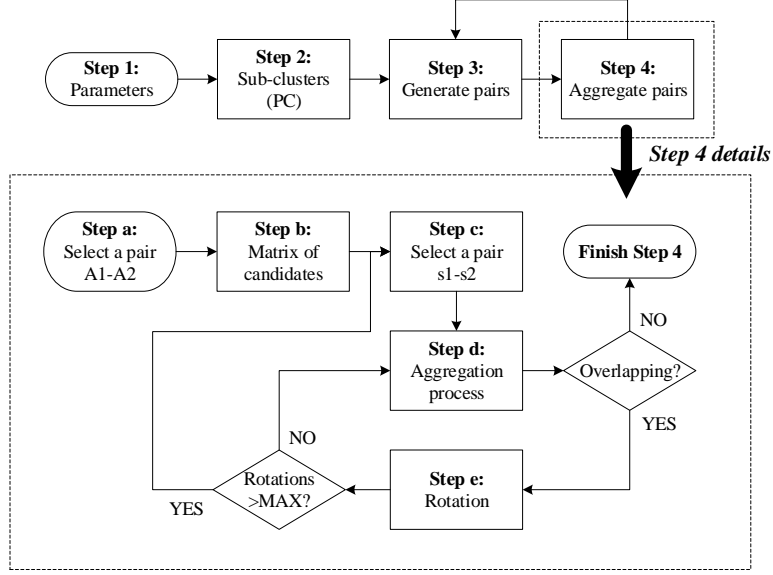


Figure 6: Flow chart of FracVAL cluster cluster aggregation algorithm.

243 unit vectors perpendicular between them and belonging to the
244 plane where the circle is embedded. All of this parameters can
245 be determined analytically as explained in Appendix B. Finally,
246 the vector $\vec{r}[\psi]$ brings^{R1.C5} the coordinates of a point belonging to
247 this circle with orientation ψ . Therefore, the work of this step
248 is reduced to just find a random angle $\psi \in [0, 2\pi]$. Subsequently,
249 the orientation of each other PP belonging to A1 is updated based in
250 the rotation of s1 by using the Euler-Rodriguez model [43].

- 251 – **Stage 3:** The location of s2 is determined by finding a random
252 point in the interception of the two spheres,^{R1.C2}

$$(r_{s1} + r_{s2})^2 = (X - X_{s1})^2 + (Y - Y_{s1})^2 + (Z - Z_{s1})^2, \quad (13a)$$

$$d_{s2}^2 = (X - X_{cm,2})^2 + (Y - Y_{cm,2})^2 + (Z - Z_{cm,2})^2, \quad (13b)$$

254 where Eq. (13a) ensures that both candidates s1 and s2 will be
255 in one point touch and Eq. (13b) ensures that candidate s2 will
256 retain their relative distance to the center of mass of aggregate

257

A2 and therefore restrictions 1 and 2 mentioned above will be fulfilled. This is illustrated in Fig. 7.^{R1.C2} One point in the in-

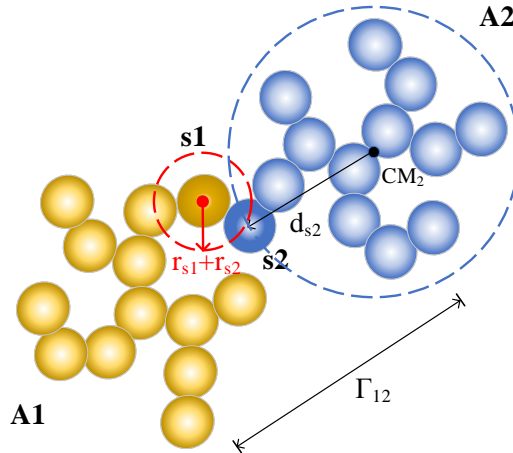


Figure 7: Intersection of spheres given by Eq. (13a) and Eq. (13b).

258

259

260

261

262

263

264

tersection of these two spheres is found using the same procedure described by equation (12). Subsequently the whole aggregate A2 is rotated based in the rotation of s2 by using the Euler-Rodriguez model [43]. At this point, restrictions 1 and 2 are ensured. Restriction 3 is not necessarily ensured, so the algorithms continue with sub-step d to check it.^{R1.C2}

265

266

267

268

269

- **Sub-step d:** Eventually, in the current orientation of A1 and A2 overlapping between PP exists. In this case the orientation of A2 is modified by random rotation by using the Euler-Rodriguez formula [43] and using the solution of the intersection of spheres given by Eq. (13a) and Eq. (13b), i.e. monomer s2 is rotated around monomer s1.

270

271

272

273

In case that overlapping still exists (following a maximum number of iteration defined by the user), the algorithm return to sub-step c and it picks another pair of monomers s1 and s2. Finally at this point, restrictions 1, 2 and 3 are ensured.

274 **4. Validation**

275 *4.1. Primary particle size distribution*

276 Figure 8 shows the histogram of primary particle radii for an aggregate
 277 consisting of $N = 1024$ primary particles sampled from a lognormal distri-
 278 bution with $\sigma_{p,geo} = 2.0$ and $r_{p,geo} = 15.0$ nm. It is evident that the specified
 279 PPSD is well preserved. When the Kolmogorov-Smirnov goodness-of-fit test
 280 (D) is applied, a value of $D = 0.03$ is obtained. A significance of $\alpha = 0.01$
 281 corresponds to a critical value of $C_{\alpha=0.01} = 0.05$. Since $D < C_{\alpha=0.01}$, the ra-
 282 dius of the primary particles of the aggregate effectively satisfies the specified
 lognormal size distribution.

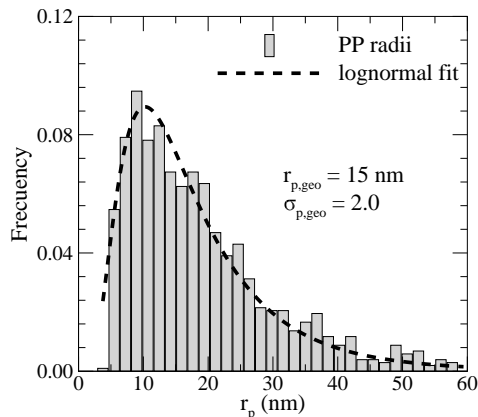


Figure 8: Histogram of radii of primary particles in an aggregate of $N = 1024$ sampled from a lognormal PPSD with $\sigma_{p,geo} = 2.0$ and $r_{p,geo} = 15.0$ nm showing the preservation of the specified distribution.

283

284 *4.2. Density-density correlation function*

285 It is expected that the spatial distribution of the mass of an aggregate
 286 should follow a specific behavior to be considered as fractal [44]. The
 287 density-density correlation function is usually examined to test if the gener-
 288 ated aggregates possess the expected fractal behavior in addition to the
 289 scaling law [45, 13]. For the particular case of aggregates formed by [R2.C5](#)
 290 polydisperse primary particles, Bushell and Amal [24] suggested to use the
 291 partial distance distribution function, which unfortunately is not practical
 292 when dealing with lognormally distributed primary particles, this because

293 there are too many different radii to obtain a partial distribution function
 294 as proposed in the mentioned reference. Therefore, we developed a new al-
 295 ternative to evaluate it. Let $f(r)$ be the density-density correlation function
 296 evaluated at a distance r from the mass center of the aggregate. This value
 297 is calculated in an iterative manner for radius in the range $r \in [R_{min}, R_{max}]$,
 298 where $R_{min} = r_{p,geo}/10$ and $R_{max} = \delta R_g$, i.e., δ times the radius of gyration
 299 of the aggregate. Normally, a value of $\delta = 3.5$ is considered sufficiently large.
 300 At the k th iteration, radius r is discretized as follows,

$$r^{(k)} = R_{min}(R_{max}/R_{min})^{k/(n_{it}-1)}. \quad (14)$$

301 where $k \in [1, (n_{it} - 1)]$, with n_{it} being a total number of discretized radii con-
 302 sidered. For a given k , a ‘‘copy’’ of the aggregate is generated and displaced
 303 at a distance $r^{(k)}$ from the mass center of the original aggregate in a random
 304 direction (i.e., a random point in a sphere). Then the volume of intersection
 305 of both aggregates $V_{int}^{(k)}$ is analytically determined based on the concept of
 306 spherical cap [46]. Hence, this process is repeated until a total of n_{or} ori-
 307 entations is evaluated. Finally, the density-density correlation function is
 308 calculated by averaging the volumes of intersection over all orientations and
 309 dividing by the total volume of the aggregate V_a ,

$$f(r^{(k)}) = \frac{1}{n_{or}} \sum_{n_{or}} V_{int}^{(k)}, \quad (15)$$

310 4.2.1. Aggregates formed by monodisperse PP

311 In Fig. 9 samples of the generated aggregates consisting of monodisperse
 312 primary particles are shown. These aggregates are generated for three dif-
 313 ferent fractal dimensions of $D_f = 1.40, 1.79,$ and 2.40 and four aggregate
 314 sizes of $N = 20, 50, 500,$ and 1024 . It is evident that a larger fractal dimen-
 315 sion leads to a more compact structure. As a way to validate our algorithm,
 316 the density-density correlation function $f(r)$ is calculated as described above
 317 considering a total of $n_{or} = 300$ orientations for each case.

318 The calculated density-density correlation functions $f(r)$ for different ag-
 319 gregate sizes from $N = 20$ up to $N = 1024$ generated using **FracVAL^{R1.C5}**
 320 and using the algorithm developed by Skorupski et al. [20] are compared in
 321 Fig. 10. It is noticed that these aggregates are generated from monodisperse
 322 primary particles.

323 The density-density correlation function $f(r)$ corresponds to the spatial
 324 mass distribution of the aggregate, and it is supposed to exhibit a slope of

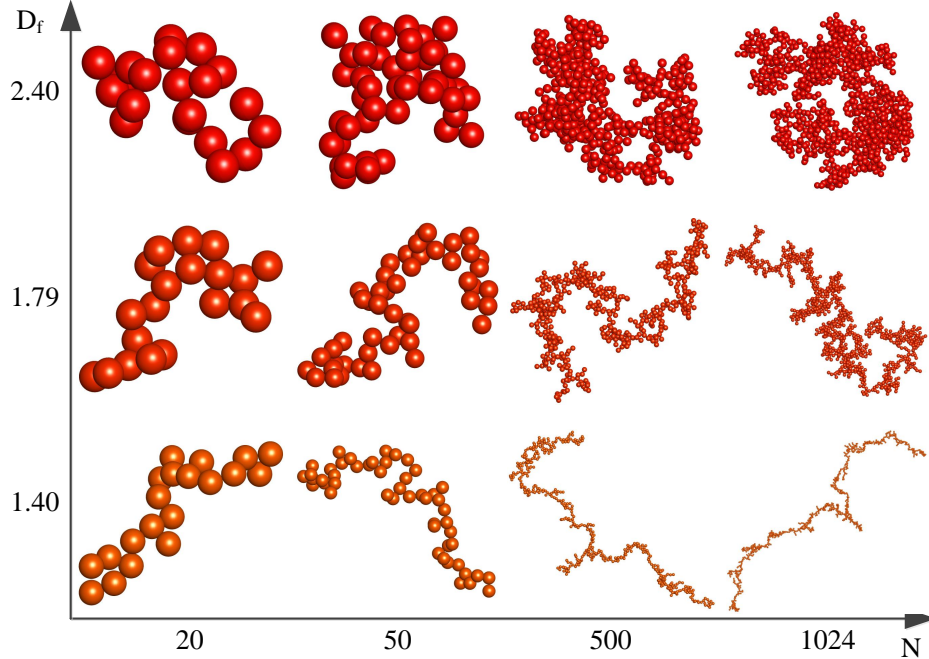


Figure 9: Selected aggregates generated by FracVAL with monodisperse PP ($\sigma_{p,geo} = 1.0$) for $D_f = 2.40$, $k_f = 0.80$ (top row), $D_f = 1.79$, $k_f = 1.40$ (middle row), and $D_f = 1.40$, $k_f = 1.80$ (bottom row).

325 $D_f - d$, where d is the Euclidean dimension of space ($d = 3$), for sufficiently
 326 large aggregates. However, due to the natural cut-off of fractal aggregates
 327 of finite size this behavior can be expected only in a limited range of r [44].
 328 As can be seen in Fig. 10, the agreement in $f(r)$ for aggregates generated
 329 from both algorithms is very good, especially for large N . In addition, the
 330 expected slope of the decay of $f(r)$ with r for sufficiently large N , i.e., $D_f - d$,
 331 is progressively displayed with increasing N , consistent with the findings of
 332 Filippov et al.^{R1.C5} [13]. As can be noted, the agreement of calculated $f(r)$
 333 with the theoretical behaviour is progressively better for larger aggregates,
 334 this is explained by the finite size effects on $f(r)$, which imply that smaller
 335 aggregates, namely $N = 20$, the $f(r)$ function is predominated by the cut-off
 336 function.^{R1.C5}

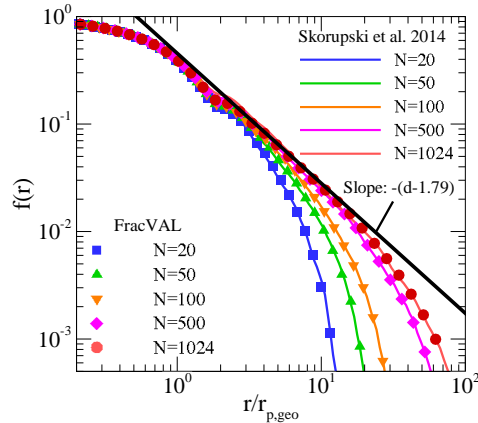


Figure 10: The density-density correlation functions of aggregates formed by monodisperse primary particles with $D_f = 1.79$, $k_f = 1.40$. The solid lines correspond to the aggregates generated by using ^{R1.C5} the algorithm of Skorupski et al. 2014 and symbols are for aggregates generated by ^{R1.C5} using FracVAL. d stands for the Euclidean dimension of space $d = 3$.

337 4.2.2. Aggregates formed by polydisperse primary particles

338 In Fig. 11 samples of aggregates formed by lognormally distributed poly-
 339 disperse primary particles with $\sigma_{p,geo} = 2.0$ using ^{R1.C5} FracVAL are shown.
 340 These aggregates are generated for $D_f = 2.60$, $k_f = 0.25$ (top row)^{R1.C5},
 341 $D_f = 1.68$, $k_f = 0.98$ (middle row), and $D_f = 1.30$, $k_f = 1.50$ ^{R1.C5} (bottom
 342 row) and for four aggregate sizes of $N = 20, 50, 500$ and 1024 .

343 Fig. 12(a) and Fig. 12(b) show the density-density correlation function
 344 of fractal aggregates of $N = 100$ and 1024 , respectively, generated using
 345 FracVAL for polydispersity levels ranging from $\sigma_{p,geo} = 1.0$ (monodisperse)
 346 to $\sigma_{p,geo} = 3.0$ (extremely polydisperse) and for different fractal properties as
 347 shown in the figure legend. As can be seen, the expected power law behavior
 348 becomes more evident, i.e., the linear decay of $f(r)$ with r in the log-log scale
 349 plot, especially for $N = 1024$. It is interesting to notice that the power law
 350 behavior seems to extend over a larger range of r for $\sigma_{p,geo} = 2$. Moreover,
 351 the slope of the calculated density-density correlation function is in good
 352 agreement with the theoretical slope of $(D_f - d)$ for all the three combinations
 353 of D_f and $\sigma_{p,geo}$, i.e., $D_f = 1.79$ and $\sigma_{p,geo} = 1.0$, $D_f = 1.68$ and $\sigma_{p,geo} = 2.0$,
 354 and $D_f = 1.48$ for $\sigma_{p,geo} = 3.0$. These values of D_f correspond to those
 355 of DLCA aggregates when considering different levels of primary particle

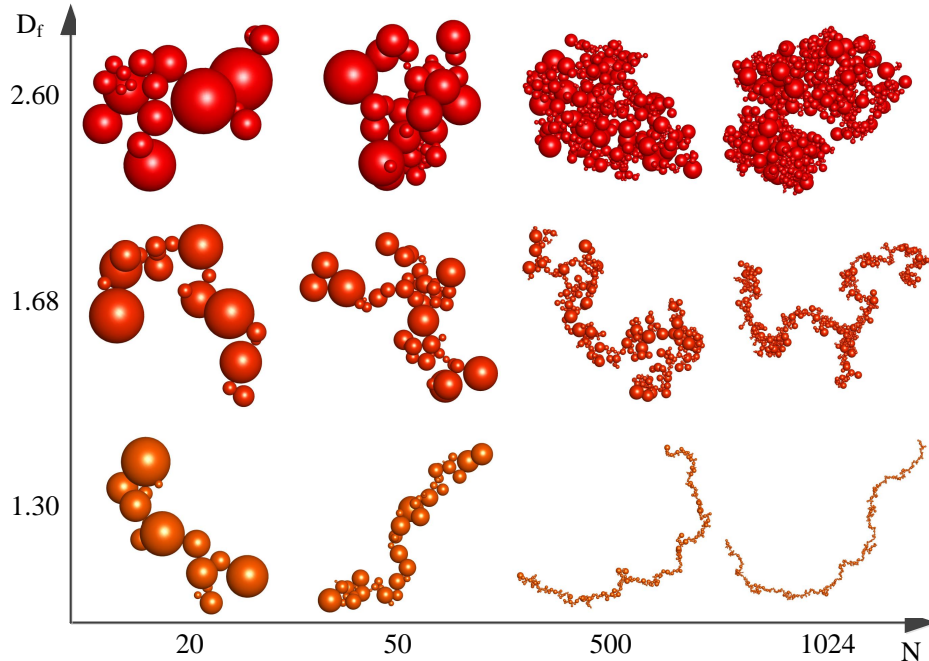


Figure 11: Sample aggregates generated by FracVAL from polydisperse $\text{PPS}^{\text{R1.C5}}$ with $\sigma_{p,geo} = 2.0$ and specified fractal parameters of $D_f = 2.60$, $k_f = 0.25$ (top row), $D_f = 1.68$, $k_f = 0.98$ (middle row), and $D_f = 1.30$, $k_f = 1.50$ (bottom row)^{R1.C5}.

356 polydispersity [21]. As expected, the agreement is better for $N = 1024$
 357 rather than $N = 100$, consistent with the results shown for monodisperse
 358 primary particles in Fig. 10.

359 4.3. Preservation of prescribed fractal parameters

360 An important feature of tunable algorithms is to ensure each individual
 361 aggregate generated accurately satisfies the scaling law expressed in Eq. (9),
 362 regardless of its size. Specifically, each individual aggregate generated by
 363 a tunable algorithm possesses the same D_f and k_f as the prescribed values.
 364 This requirement is naturally built into the algorithm through the application
 365 of Eq. (9) during the generation.

366 To probe the preservation of fractal parameters (D_f and k_f) on a global
 367 sense, i.e., to examine an ensemble of aggregates of different sizes, plots of
 368 $\log(N) - \log(R_g/r_{p,geo})$ for different prescribed fractal dimension and pref-

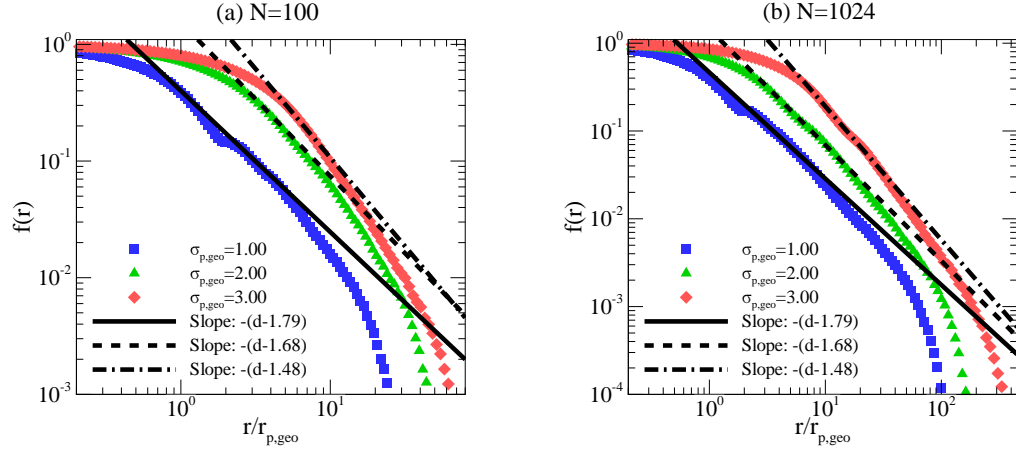


Figure 12: The calculated density-density correlation functions of aggregates consisting of $N = 100$, $N = 1024$ primary particles of different levels of polydispersity. The imposed fractal parameters are: $D_f = 1.79$, $k_f = 1.40$ for $\sigma_{p,geo} = 1.0$, $D_f = 1.68$, $k_f = 0.98$ for $\sigma_{p,geo} = 2.0$, and $D_f = 1.48$, $k_f = 0.77$ for $\sigma_{p,geo} = 3.0$. d stands for the Euclidean dimension of space with $d = 3$.

369 actor are presented in Fig. 13(a) and 13(b) for monodisperse ($\sigma_{p,geo} = 1$)
 370 and polydisperse ($\sigma_{p,geo} = 2$) primary particles, respectively. The aggregate
 371 size is varied non-uniformly from $N = 20$ to 1024. It is important to note
 372 that each data point in Fig. 13 corresponds to 50 aggregates. As observed in
 373 the figure, each condition for individual aggregates (characterized by D_f , k_f ,
 374 N , and $\sigma_{p,geo}$) accurately preserves the prescribed fractal parameters. The
 375 solid lines represent the log-log fit of the data points and the corresponding
 376 parameters are reported in the figure legend. It is evident that all the curves
 377 display a linear variation of N with the normalized R_g in the log-log plot
 378 expected from the scaling law of Eq. (3).

379 As can be seen in Fig. 13(a) for all three sets of aggregates formed by
 380 monodisperse primary particles, the fractal scaling law is very accurately pre-
 381 served and the fractal dimension based on the slope of the linear fit deviates
 382 from the prescribed value by less than only 1%. The same observations can
 383 be made for aggregates formed polydisperse primary particles as shown in
 384 Fig. 13(b). It is worth pointing out that these pairs of D_f and k_f are selected
 385 to represent the most extreme values under which FracVAL is able to gener-
 386 ate the fractal aggregates for the evaluated PP polydispersity ($\sigma_{p,geo} = 2$).
 387 The results shown in Fig. 13 confirm that the ensemble of aggregates gener-

388 ated by FracVAL strictly preserves the prescribed fractal parameters under
 389 different conditions in terms of fractal parameters (D_f and k_f) and the level
 390 of primary particle polydispersity as long as the fractal aggregates can be
 generated by FracVAL.

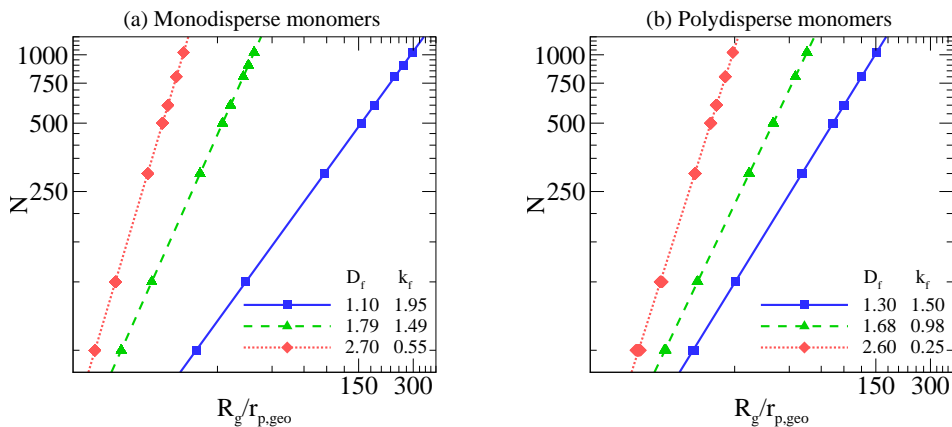


Figure 13: Preservation of fractal parameters for aggregates consisting of (a) monodisperse ($\sigma_{p,geo} = 1$) and (b) polydisperse ($\sigma_{p,geo} = 2$) primary particles for different combinations of fractal parameters (D_f and k_f). Continuous lines represent the log-log fit of the points, corresponding parameters are reported in the legend of the figures.

391

392 Once these aggregates are generated, numerical projections, like numerical
 393 TEM images [46], could be generated in order to relate the projected
 394 density-density correlation function as calculated by Nelson et al. [47] for nu-
 395 merically generated aggregates in comparison with experimentally measured
 396 ones. This feature will be available in a future version of FracVAL.^{R1.C3}

397 5. Discussion

398 To demonstrate the advantage of FracVAL algorithm over the classical
 399 Filippov et al. [13] one, Fig. 14 compares the plots of $\log(N)$ as a function
 400 $\log(R_g/r_{p,geo})$ in log-log scale for aggregates generated using FracVAL and a
 401 direct application of the Filippov et al. [13]^{R1.C4} algorithm for polydisperse
 402 primary particles. The prescribed parameters are $D_f = 1.68$, $k_f = 0.98$,
 403 and $\sigma_{p,geo} = 2.0$ and for aggregate sizes from $N = 20$ to 1024. It is noticed
 404 that in the Filippov et al. [13] method considered Eq. (7) instead of the
 405 derived Eq. (6), which is used in FracVAL. Therefore, the effect of primary
 406 particle polydispersity on aggregate center of mass and radius of gyration

407 is not taken into account in the formulation of Filippov et al. [13]^{R1.C4} It
 408 is also worth pointing out that the FLAGE algorithm recently developed
 409 by Skorupski et al. [20] also made a direct application of the Filippov et
 410 al. [13]^{R1.C4} method for aggregates formed polydisperse primary particles
 411 and the results of Filippov et al. [13]^{R1.C4} shown in Fig. 14^{R1.C4} should be
 412 identical to the results of FLAGE.

413 A total of 200 aggregates is generated using the method of Filippov et
 414 al. [13] for each set of parameters (D_f , k_f , N , and $\sigma_{p,geo}$). As can be seen,
 415 when primary particles are polydisperse, the classical Filippov et al. [13] does
 416 not preserve exactly the fractal parameters (D_f and k_f) for each individual
 417 aggregate, though the fractal parameters are preserved on an ensemble basis.
 418 Therefore, a large population of aggregates should be generated if one uses the
 419 Filippov et al. [13]^{R1.C4} method or the FLAGE code to generate aggregates
 420 formed by polydisperse primary particles. It is interesting to observe that the
 421 scatter of $\log(R_g/r_{p,geo})$ at a given N becomes increasingly smaller and the
 422 agreement between Filippov et al. [13] and FracVAL^{R1.C5} is improved with
 423 increasing N . This agreement is employed in previous studies presented in
 the literature [46, 32].

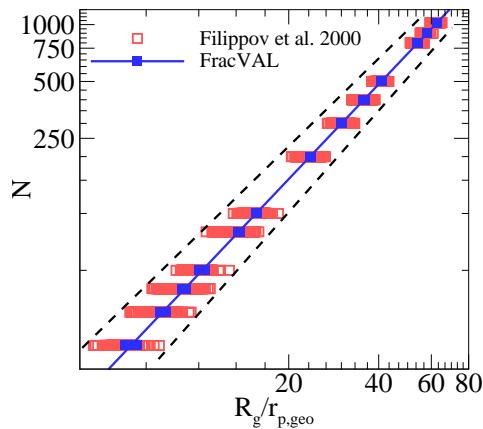


Figure 14: Comparison of results by using Filippov et al. [13] method and FracVAL. Aggregates consisting of $D_f = 1.68$ and $k_f = 0.98$ and $\sigma_{p,geo} = 2.0$.

424 Finally, the computational performance of the FracVAL algorithm is eval-
 425 uated. The computations are carried out using a laptop equipped with a 2.40
 426 GHz CPU and 8 Gb of memory. The reported CPU times are averaged over
 427

428 a population of 100 aggregates for different combinations of D_f and k_f within
429 the range of $D_f = 1.0 - 3.0$ and k_f between 0.1 and 2.4. The computational
430 time is dependent on the number of monomers, the level of primary particle
431 polydispersity, and the combination of D_f and k_f . Table 1 presents exam-
432 ples of average time required to generate an aggregate consisting of $N = 500$
433 for monomers polydispersity from $\sigma_{p,geo} = 1.0$ to 3.0. All examples of ag-
434 gregates consisting of 500 PPs^{R2.C4} are generated in less than 2.4 minutes.
435 Meanwhile aggregates consisting of 1000 PPs are generated in less than 14
436 minutes. Generation of aggregates formed by polydisperse PPs is generally
437 more time-consuming than those formed by monodisperse PPs.^{R2.C4} It is im-
438 portant to remark that the majority of times is in the order of the minimum
439 values reported in Table 1, while the maximum values are achieved only for
440 combinations of extremely different D_f and k_f pairs and also these max-
441 imum times exhibit a much larger standard deviation than the minimum
values.^{R2.C4}

Table 1: Assessment of the average computational time (in seconds) required by FracVAL.

$\sigma_{p,geo}$	$N = 500$ ^{R2.C4}	$N = 1000$ ^{R2.C4}
1.00	1.1-70.1	5.3-84.6 ^{R2.C4}
1.45	1.9-73.6	8.9-408 ^{R2.C4}
2.00	3.9-145.8	28.2-791.1 ^{R2.C4}
2.50	5.6-15.1	37.6-113.7 ^{R2.C4}
3.00	7.0-9.4	38-74.6 ^{R2.C4}

442

443 6. Conclusions

444 A novel tunable cluster-cluster aggregation algorithm, FracVAL, is devel-
445 oped in this study to numerically generate fractal aggregates formed by poly-
446 disperse primary particles. The algorithm represents an **improvement**^{R2.C4} of
447 the tunable cluster-cluster aggregation algorithm of Filippov et al. [13] for
448 generation of fractal aggregates formed by monodisperse primary particles.
449 The algorithm is validated by comparing the density-density correlation func-
450 tions of fractal aggregates generated by FracVAL and a literature method,
451 FLAGE [20], and excellent agreement is observed. The prescribed fractal
452 parameters D_f and k_f are found accurately preserved for each individual ag-
453 gregate consisting of either monodisperse or polydisperse primary particles.
454 The fractal properties of an ensemble of aggregates of different sizes are also

455 found to accurately preserve the prescribed D_f and k_f with less than 1%
456 deviation for different combinations of D_f and k_f , regardless of the degree of
457 primary particle polydispersity characterized by $\sigma_{p,geo}$ up to 3.

458 Since the positions of the two aggregating primary particles and the mass
459 centers of the two aggregating clusters are found using analytical expressions
460 by using the intersection of two spheres and random parameters, FracVAL
461 is considerably computationally efficient for generating fractal aggregates for
462 different combinations of D_f , k_f , and $\sigma_{p,geo}$ for $\sigma_{p,geo}$ up to 3, taking in average
463 less than 2.4 minutes for $N = 500$ and 14 minutes for $N = 1000$ PPs^{R2.C4}
464 on a regular laptop, as long as the pair of D_f and k_f falls in the valid range
465 where it is possible to generate such fractal aggregates.

466 Finally, it is demonstrated that the direct use of the tunable cluster-
467 cluster aggregation algorithm Filippov et al. [13] to generate aggregates
468 formed by polydisperse primary particles, such as implemented in the FLAGE
469 code, does not preserve the prescribed fractal properties (D_f and k_f) for in-
470 dividual aggregates, though it does so globally, i.e., the fractal properties of
471 an ensemble of aggregates recover the prescribed values. This observation
472 suggests that caution should be taken when a certain property of individual
473 aggregates formed by polydisperse primary particles generated by FLAGE is
474 investigated, since the fractal dimension or prefactor may be different from
475 the expected value. On the other hand, the algorithm developed in this study,
476 FracVAL, overcomes the drawback of the Filippov et al. [13]^{R1.C4} method and
477 the FLAGE code.

478 Acknowledgments

479 This work is supported by the Chilean CONICYT Research programs
480 under Grant FONDECYT project 1161453 and partially by PIA-Anillo CyT
481 project ACT172095.

482 References

- 483 [1] F. Babick, Suspensions of colloidal aggregates, in: Suspensions of Col-
484 loidal Particles and Aggregates, Springer, 2016, pp. 119–220.
485 URL https://doi.org/10.1007/978-3-319-30663-6_4
- 486 [2] T. A. Witten, L. M. Sander, Phys. Rev. Lett. 47 (1981) 1400–1403.
487 [link].
488 URL <https://doi.org/10.1103/PhysRevLett.47.1400>

- 489 [3] P. Meakin, Phys. Rev. Lett. 51 (1983) 1119–1122. [link].
490 URL <https://doi.org/10.1103/PhysRevLett.51.1119>
- 491 [4] M. Kolb, R. Botet, R. Jullien, Phys. Rev. Lett. 51 (1983) 1123–1126.
492 [link].
493 URL <https://doi.org/10.1103/PhysRevLett.51.1123>
- 494 [5] R. C. Ball, T. A. Witten, Phys. Rev. A 29 (1984) 2966–2967. [link].
495 URL <https://doi.org/10.1103/PhysRevA.29.2966>
- 496 [6] S. Tolman, P. Meakin, Phys. Rev. A 40 (1989) 428–437. [link].
497 URL <https://doi.org/10.1103/PhysRevA.40.428>
- 498 [7] P. Meakin, J. Sol-Gel Sci. Technol. 15 (2) (1999) 97–117. [link].
499 URL <https://doi.org/10.1023/A:1008731904082>
- 500 [8] F. Braga, M. S. Ribeiro, Comput. Phys. Commun. 182 (8) (2011) 1602
501 – 1605. [link].
502 URL <https://doi.org/10.1016/j.cpc.2011.04.005>
- 503 [9] K. R. Kuijpers, L. de Martín, J. R. van Ommen, Comput. Phys. Com-
504 mun. 185 (3) (2014) 841–846. [link].
505 URL <https://doi.org/10.1016/j.cpc.2013.12.003>
- 506 [10] C. Li, H. Xiong, Comput. Phys. Commun. 185 (12) (2014) 3424–3429.
507 [link].
508 URL <https://doi.org/10.1016/j.cpc.2014.08.017>
- 509 [11] R. Thouy, R. Jullien, J. Phys. A: Math. Gen. 27 (9) (1994) 2953–2963.
510 [link].
511 URL <https://doi.org/10.1088/0305-4470/27/9/012>
- 512 [12] D. W. Mackowski, Appl. Opt. 34 (18) (1995) 3535–45. [link].
513 URL <https://doi.org/10.1364/AO.34.003535>
- 514 [13] A. Filippov, M. Zurita, D. Rosner, J. Colloid Interface Sci. 229 (1) (2000)
515 261–273. [link].
516 URL <https://doi.org/10.1006/jcis.2000.7027>
- 517 [14] U. Kätzel, R. Bedrich, M. Stintz, R. Ketzmerick, T. Gottschalk-Gaudig,
518 H. Barthel, Part. Part. Syst. Char. 25 (1) (2008) 9–18. [link].
519 URL <https://doi.org/10.1002/ppsc.200700004>

- 520 [15] R. K. Chakrabarty, M. A. Garro, S. Chancellor, C. Herald,
521 H. Moosmüller, *Comput. Phys. Commun.* 180 (8) (2009) 1376–1381.
522 doi:<https://doi.org/10.1016/j.cpc.2009.01.026>.
- 523 [16] C. Ringl, H. M. Urbassek, *Comput. Phys. Commun.* 184 (7) (2013)
524 1683–1685. [link].
525 URL <https://doi.org/10.1016/j.cpc.2013.02.012>
- 526 [17] L. Ehrl, M. Soos, M. Lattuada, *J. Phys. Chem. B* 113 (31) (2009) 10587–
527 10599. [link].
528 URL <https://doi.org/10.1021/jp903557m>
- 529 [18] S. Prasanna, P. Rivière, A. Soufiani, *J. Quant. Spectrosc. Radiat. Trans-*
530 *fer* 148 (2014) 141 – 155. [link].
531 URL <https://doi.org/10.1016/j.jqsrt.2014.07.004>
- 532 [19] A. D. Melas, L. Isella, A. G. Konstandopoulos, Y. Drossinos, *J. Colloid*
533 *Interface Sci.* 417 (2014) 27 – 36. [link].
534 URL <https://doi.org/10.1016/j.jcis.2013.11.024>
- 535 [20] K. Skorupski, J. Mroczka, T. Wriedt, N. Riefler, *Physica A* 404 (2014)
536 106–117. [link].
537 URL <https://doi.org/10.1016/j.physa.2014.02.072>
- 538 [21] M. L. Eggersdorfer, S. E. Pratsinis, *Aerosol Sci. Technol.* 46 (3) (2012)
539 347–353. [link].
540 URL <https://doi.org/10.1080/02786826.2011.631956>
- 541 [22] R. Dastanpour, S. N. Rogak, *J. Aerosol Sci.* 94 (2016) 22–32. [link].
542 URL <https://doi.org/10.1016/j.jaerosci.2015.12.005>
- 543 [23] M. Tence, J. P. Chevalier, R. Jullien, *J. Physique* 47 (11) (1986) 1989–
544 1998. [link].
545 URL <https://doi.org/10.1051/jphys:0198600470110198900>
- 546 [24] G. Bushell, R. Amal, *J. Colloid Interface Sci.* 205 (2) (1998) 459–469.
547 [link].
548 URL <https://doi.org/10.1006/jcis.1998.5667>
- 549 [25] G. Bushell, R. Amal, *J. Raper, Part. Part. Syst. Char.* 15 (1998) 3–8.
550 [link].
551 URL [https://doi.org/10.1002/\(SICI\)1521-4117\(199802\)15:1<3::AID-PPSC3>3.0.CO;2](https://doi.org/10.1002/(SICI)1521-4117(199802)15:1<3::AID-PPSC3>3.0.CO;2)

- 552 [26] T. L. Farias, Ü. Ö. Köylü, M. G. Carvalho, J. Quant. Spectrosc. Radiat.
553 Transfer 55 (3) (1995) 357–371. [link].
554 URL [https://doi.org/10.1016/0022-4073\(95\)00166-2](https://doi.org/10.1016/0022-4073(95)00166-2)
- 555 [27] T. Seto, A. Hirota, T. Fujimoto, M. Shimada, K. Okuyama, Aerosol Sci.
556 Technol. 27 (3) (1997) 422–438. [link].
557 URL <https://doi.org/10.1080/02786829708965482>
- 558 [28] T. T. Charalampopoulos, G. Shu, Appl. Opt. 41 (4) (2002) 723–733.
559 [link].
560 URL <https://doi.org/10.1364/AO.41.000723>
- 561 [29] F. Liu, M. Yang, F. Hill, D. Snelling, G. Smallwood, Appl. Phys. B
562 83 (3) (2006) 383. [link].
563 URL <https://doi.org/10.1007/s00340-006-2196-z>
- 564 [30] M. C. Heine, S. E. Pratsinis, J. Aerosol Sci. 38 (1) (2007) 17–38. [link].
565 URL <https://doi.org/10.1016/j.jaerosci.2006.09.005>
- 566 [31] J. Y. Yin, L. H. Liu, J. Quant. Spectrosc. Radiat. Transfer 111 (14)
567 (2010) 2115–2126. [link].
568 URL <https://doi.org/10.1016/j.jqsrt.2010.05.016>
- 569 [32] C. Liu, Y. Yin, F. Hu, H. Jin, C. M. Sorensen, Aerosol Sci. Technol.
570 49 (10) (2015) 928–940. [link].
571 URL <https://doi.org/10.1080/02786826.2015.1085953>
- 572 [33] E. Goudeli, M. L. Eggersdorfer, S. E. Pratsinis, Langmuir 32 (36) (2016)
573 9276–9285. [link].
574 URL <https://doi.org/10.1021/acs.langmuir.6b02455>
- 575 [34] J. Yon, F. Liu, J. Morán, A. Fuentes, Proc. Combust. Inst.[link].
576 URL <https://doi.org/10.1016/j.proci.2018.07.065>
- 577 [35] A. Spyrogianni, K. S. Karadima, E. Goudeli, V. G. Mavrantzas, S. E.
578 Pratsinis, J. Chem. Phys. 148 (6) (2018) 064703. [link].
579 URL <https://doi.org/10.1063/1.5012037>
- 580 [36] A. Bescond, J. Yon, F. X. Ouf, D. Ferry, D. Delhaye, D. Gaffié, A. Cop-
581 palle, C. Rozé, Aerosol Sci. Technol. 48 (8) (2014) 831–841. [link].
582 URL <https://doi.org/10.1080/02786826.2014.932896>

- 583 [37] D. Boldridge, *Aerosol Sci. Technol.* 44 (3) (2010) 182–186. [link].
584 URL <https://doi.org/10.1080/02786820903499462>
- 585 [38] S. Bau, O. Witschger, F. Gensdarmes, O. Rastoix, D. Thomas, *Powder*
586 *Technol.* 200 (3) (2010) 190–201. [link].
587 URL <https://doi.org/10.1016/j.powtec.2010.02.023>
- 588 [39] D. Cortés, J. Morán, F. Liu, F. Escudero, J.-L. Consalvi, A. Fuentes,
589 *Energy Fuels* 32 (11) (2018) 11802–11813. [link].
590 URL <https://doi.org/10.1021/acs.energyfuels.8b01301>
- 591 [40] C. M. Sorensen, G. D. Feke, *Aerosol Sci. Technol.* 25 (3) (1996) 328–337.
592 [link].
593 URL <https://doi.org/10.1080/02786829608965399>
- 594 [41] C. Forbes, M. Evans, N. Hastings, B. Peacock, *Statistical distributions*,
595 John Wiley & Sons, 2011.
- 596 [42] C. M. Sorensen, C. Oh, *Phys. Rev. E* 58 (1998) 7545–7548. [link].
597 URL <https://doi.org/10.1103/PhysRevE.58.7545>
- 598 [43] J. S. Dai, *Mech. Mach. Theory* 92 (2015) 144–152. [link].
599 URL <https://doi.org/10.1016/j.mechmachtheory.2015.03.004>
- 600 [44] R. Jullien, *Contemp. Phys.* 28 (5) (1987) 477–493. [link].
601 URL <https://doi.org/10.1080/00107518708213736>
- 602 [45] A. Hasmy, M. Foret, J. Pelous, R. Jullien, *Phys. Rev. B* 48 (13) (1993)
603 9345. [link].
604 URL <https://doi.org/10.1103/PhysRevB.48.9345>
- 605 [46] J. Morán, J. Cuevas, F. Liu, J. Yon, A. Fuentes, *Powder Technol.* 330
606 (2018) 67 – 79. [link].
607 URL <https://doi.org/10.1016/j.powtec.2018.02.008>
- 608 [47] J. A. Nelson, R. J. Crookes, S. Simons, *J. Phys. D* 23 (4) (1990) 465.
609 [link].
610 URL <http://stacks.iop.org/0022-3727/23/i=4/a=014>

611 **Appendix A. Derivation of Eq.(6)**

612 The resulting center of mass (R_c) of an aggregate formed by the aggre-
 613 gation of two clusters of N_1 and N_2 PPs with mass m_1 and m_2 , respectively
 614 is,

$$mR_c = \sum_{i=1}^N m_{p,i}R_i = \sum_{j=1}^{N_1} m_{p,j}R_j + \sum_{k=1}^{N_2} m_{p,k}R_k, \quad (\text{A.1})$$

615 where $N_1 + N_2 = N$ and $m_1 + m_2 = m$. Therefore,

$$mR_c = m_1R_{c1} + m_2R_{c2}. \quad (\text{A.2})$$

616 Let's Γ be the vector that stands for the distance between the center of
 617 mass of the two sub-clusters,

$$\Gamma = R_{c2} - R_{c1}, \quad (\text{A.3})$$

618 getting m_1 and m_2 from the relation $m = m_1 + m_2$ and replacing their
 619 values in Eq. (A.2) we can obtain,

$$R_{c1} - R_c = -\frac{m_2}{m}\Gamma, \quad (\text{A.4a})$$

$$R_{c2} - R_c = \frac{m_1}{m}\Gamma, \quad (\text{A.4b})$$

620 On the other hand, from the radius of gyration of the original aggregate
 621 calculated from Eq. (4) we obtain,

$$m^2R_g^2 = \sum_{j=1}^{N_1} m_{p,j} [(R_j - R_{c1} + R_{c1} - R_c)^2 + r_{g,p,j}^2] + \sum_{k=1}^{N_2} m_{p,k} [(R_k - R_{c2} + R_{c2} - R_c)^2 + r_{g,p,k}^2], \quad (\text{A.5})$$

$$m^2R_g^2 = \sum_{j=1}^{N_1} m_{p,j} [(R_j - R_{c1})^2 + r_{g,p,j}^2 + 2(R_j - R_{c1})(R_{c1} - R_c)] + \sum_{k=1}^{N_2} m_{p,k} [(R_k - R_{c2})^2 + r_{g,p,k}^2 + 2(R_k - R_{c2})(R_{c2} - R_c)] + m_1(R_{c1} - R_c)^2 + m_2(R_{c2} - R_c)^2, \quad (\text{A.6})$$

622 where the terms: $\sum_{j=1}^{N_1} 2m_{p,j}(R_j - R_{c1})(R_{c1} - R_c)$ and $\sum_{k=1}^{N_2} 2m_{p,k}(R_k -$
 623 $R_{c2})(R_{c2} - R_c)$ are both equal to zero.

$$m^2 R_g^2 = \sum_{j=1}^{N_1} m_{p,j} [(R_j - R_{c1})^2 + r_{g,p,j}^2] + m_1 (R_{c1} - R_c)^2 + \sum_{k=1}^{N_2} m_{p,k} [(R_k - R_{c2})^2 + r_{g,p,k}^2] + m_2 (R_{c2} - R_c)^2, \quad (\text{A.7})$$

624 combining this result with Eq. (A.4a) and Eq. (A.4b) and introducing R_{g1}
625 and R_{g2} as the radius of gyration of both sub-clusters we get,

$$m^2 R_g^2 = m (m_1 R_{g1}^2 + m_2 R_{g2}^2) + \Gamma^2 m_1 m_2, \quad (\text{A.8})$$

626 if we consider the particular case of aggregates consisting of monodisperse
627 PPs with mass m_p , consequently $m = N m_p$, $m_1 = N_1 m_p$ and $m_2 = N_2 m_p$,
628 then Eq. (6) turns to,

$$N^2 R_g^2 = N (N_1 R_{g1}^2 + N_2 R_{g2}^2) + \Gamma^2 N_1 N_2, \quad (\text{A.9})$$

629 which is equivalent to the relationship derived by Filippov et al. [13].

630 Appendix B. Sphere-sphere intersection

631 Lets consider two spheres in \mathfrak{R}^3 with equations,

$$(x - x_1)^2 + (y - y_1)^2 + (z - z_1)^2 = r_1^2, \quad (\text{B.1a})$$

$$(x - x_2)^2 + (y - y_2)^2 + (z - z_2)^2 = r_2^2. \quad (\text{B.1b})$$

633 Lets d be the distance between the center of the two spheres. Based in
634 the law of cosines,

$$\cos[\alpha] = \frac{-r_2^2 + r_1^2 + d^2}{2r_1 d}, \quad (\text{B.2})$$

635 The intersection of these two spheres is a circle contained in the plane of
636 intersection. Lets ρ be the radius of this circle, then $\rho = r_1 \sin[\alpha]$, considering
637 Eq. (B.2) and the identity $\sin^2[\alpha] + \cos^2[\alpha] = 1$ we obtain,

$$\rho = \frac{1}{2d} \sqrt{4r_1^2 d^2 - (-r_2^2 + r_1^2 + d^2)^2}. \quad (\text{B.3})$$

638 On the other hand, the plane of intersection is obtained by subtracting
639 Eq. (B.1a) and Eq. (B.1b) by considering $A = 2(x_2 - x_1)$, $B = 2(y_2 - y_1)$,
640 $C = 2(z_2 - z_1)$ and $D = (r_1^2 - r_2^2) + (x_2^2 - x_1^2) + (y_2^2 - y_1^2) + (z_2^2 - z_1^2)$,

$$Ax + By + Cz = D. \quad (\text{B.4})$$

641 The equation of the line that connect the centers of the two spheres is,

$$x = x_1 + t(x_2 - x_1), \quad y = y_1 + t(y_2 - y_1), \quad z = z_1 + t(z_2 - z_1), \quad (\text{B.5})$$

642 The intersection of this line and the plane given by Eq. (B.4) bring us
643 the value of the constant t as following,

$$t = \frac{Ax_1 + By_1 + Cz_1 - D}{A(x_1 - x_2) + B(y_1 - y_2) + C(z_1 - z_2)}, \quad (\text{B.6})$$

644 replacing in Eq. (B.5) we obtain the coordinates \vec{c} of the center of the
645 circle of intersection between the two spheres. Finally, with the coordinates
646 of the center \vec{c} and the radius ρ , the equation of the circle of intersection of
647 the two spheres can be parametrized as follows,

$$\vec{r}[\psi] = \vec{c} + \rho \cos[\psi] \hat{i}' + \rho \sin[\psi] \hat{j}', \quad \psi \in [0, 2\pi] \quad (\text{B.7})$$

648 where \hat{i}' and \hat{j}' are two perpendicular unit vectors belonging to the plane
649 given by Eq. (B.4).

650 **Appendix C. Sensitivity analysis to initial sub-clusters morphol-** 651 **ogy and size**

652 We intend to answer the following question: how important are the ini-
653 tial sub-clusters to the final aggregates generated with FracVAL? To this end
654 a sensitivity analysis of the density pair-correlation function $f(r)$ is carried
655 out. For aggregates consisting of $N = 100$ monomers a sensitivity analysis
656 is developed for monodisperse (Fig. C.15(a) and Fig. C.15(b)) and poly-
657 disperse (Fig. C.15(c) and Fig. C.15(d)) primary particles. A total of 3
658 parameters are varied. In Fig. C.15(a) and Fig. C.15(c) the sensitivity of
659 the density pair-correlation function $f(r)$ to the size of initial sub-clusters is
660 tested considering $N_{sub} = 5, 10$ and 15% (expressed in a percentage of N).
661 The other two parameters considered are the fractal dimension and prefactor
662 used for the generation of sub-clusters. The sensitivity of the density pair-
663 correlation function $f(r)$ to D_f and k_f with a variation of $\pm 20\%$ is reported
664 in Fig. C.15(b) and Fig. C.15(d) for monodisperse and polydisperse PPs,

665 respectively. Please note that in the latter cases only the fractal parameters
666 of the sub-clusters are varied meanwhile those corresponding to the final
667 aggregate remain constant (fixed to the original imposed D_f and k_f). As
668 expected, for all cases consisting of monodisperse PPs there is no variation
669 for $r/r_{p,geo} \leq 2$, because at this scale only intersection between equally sized
670 spheres is found. For larger ranges $r/r_{p,geo} > 2$ the overall behaviour of the
671 pair correlation function is not significantly affected by the three concerned
672 parameters except in the polydisperse PPs case when the fractal dimension of
673 the sub-cluster is strongly modified ($\pm 20\%$). Nevertheless, the effect seems
674 limited to the domain of $r/r_{p,geo} \in [2, 8]$.

675 **Appendix D. Further explanation of cases 2 and 3 of section 3.2**

676 In the context of Section 3.2 in sub-step 4b we identified 3 possible cases of
677 aggregation of two sub-clusters A1 and A2. The main part of the manuscript
678 is devoted to explain Case 1 for being considered as the most common case.
679 This appendix intends to provide a detailed explanation of Cases 2 and 3.

- 680 • Case 2: When the sphere of radius $D_{i1,+}$ is large to enclose the sphere
681 of radius $D_{j2,+}$, i.e., when $(D_{i1,+} - D_{j2,+}) > \Gamma_{12}$ with an upper limit
682 $D_{i1,-} \leq \Gamma_{12} + D_{j2,+}$. Please see Fig. D.16.
- 683 • Case 3: Analogously, when the sphere of radius $D_{j2,+}$ is large to enclose
684 the sphere of radius $D_{i1,+}$, i.e., when $(D_{j2,+} - D_{i1,+}) > \Gamma_{12}$ with an
685 upper limit $D_{j2,-} \leq \Gamma_{12} + D_{i1,+}$.

686 In the context of sub-step 4c, there are three different scenarios for joining
687 the sub-cluster A1 and A2 by selecting the candidate primary particles s1
688 (belonging to A1) and s2 (belonging to A2). Therefore, we will be concerned
689 about the following spheres,

$$690 \text{ Sph.1 : } D_{s1,+}^2 = (X - X_{cm,1})^2 + (Y - Y_{cm,1})^2 + (Z - Z_{cm,1})^2, \quad (\text{D.1a})$$

$$691 \text{ Sph.2 : } D_{s1,-}^2 = (X - X_{cm,1})^2 + (Y - Y_{cm,1})^2 + (Z - Z_{cm,1})^2, \quad (\text{D.1b})$$

$$692 \text{ Sph.3 : } D_{s2,+}^2 = (X - X_{cm,2})^2 + (Y - Y_{cm,2})^2 + (Z - Z_{cm,2})^2, \quad (\text{D.1c})$$

$$693 \text{ Sph.4 : } D_{s2,-}^2 = (X - X_{cm,2})^2 + (Y - Y_{cm,2})^2 + (Z - Z_{cm,2})^2. \quad (\text{D.1d})$$

694 The reason that many spheres appear is that the possible solutions, i.e.,
the intersections between s1 and s2, correspond to the intersection of two

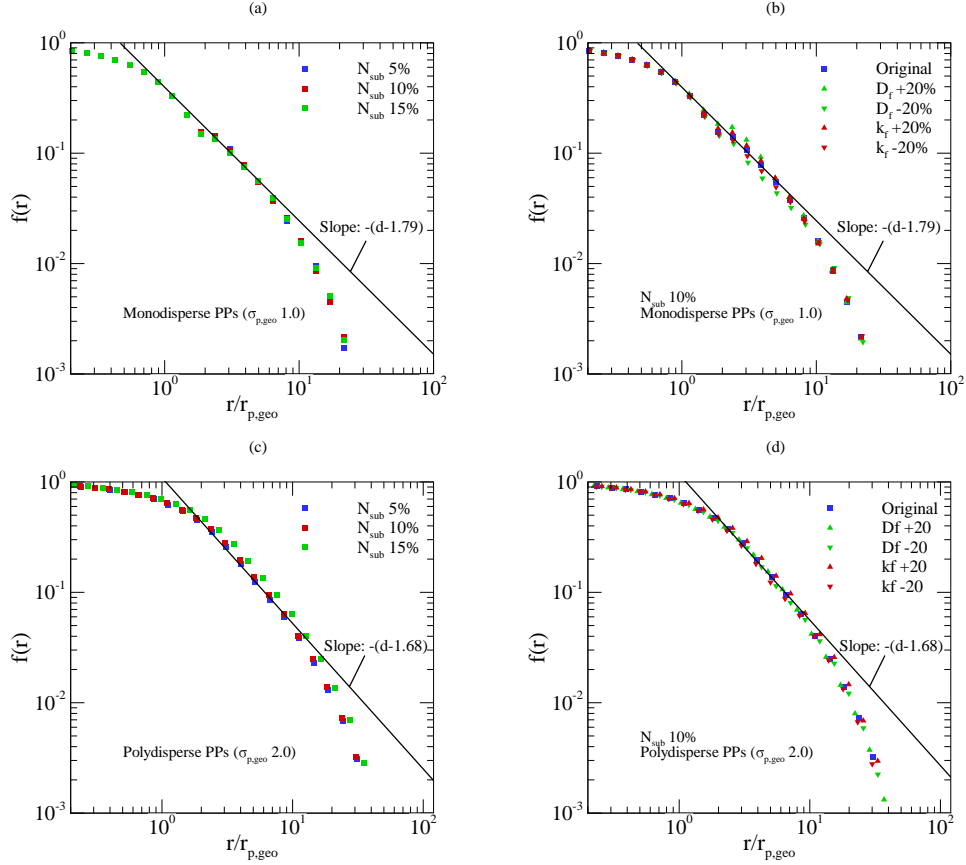


Figure C.15: Sensitivity analysis of density-density correlation function for the initial sub-clusters consisting of monodisperse (a and b) and polydisperse PPs (Figs. c and d). Figs. (a) and (c) illustrate the sensitivity of the initial sub-clusters size (N_{sub}), and Figures (b) and (d) show the sensitivity to fractal parameters (D_f and k_f). All aggregates consist of $N = 100$ monomers, fractal parameters $D_f = 1.79$ and $k_f = 1.40$ for monodisperse ($\sigma_{p,geo} = 1$) and $D_f = 1.68$ and $k_f = 0.98$ for polydisperse PPs ($\sigma_{p,geo} = 2$).

695 spherical shells. The spherical shell belonging to A1 is determined by the
 696 concentric spheres Sph.1 and Sph.2 and the spherical shell belonging to A2
 697 is analogously determined by the spheres Sph.3 and Sph.4. The above men-
 698 tioned 3 possible scenarios are described as follows,

- 699 • Please note that the intersection of spheres 2 and 4 is not possible and
 700 therefore it does not lead to any possible solution.
- 701 • Scenario 1: When $\Gamma_{12} \geq |D_{s1,+} - D_{s2,+}|$. In this case (considered

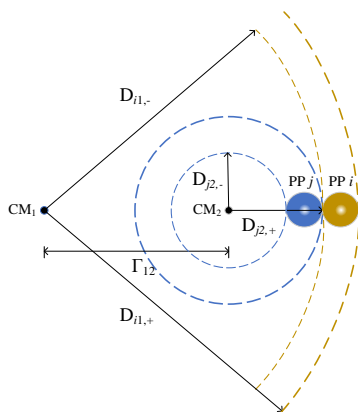


Figure D.16: Limiting candidate for Case 2 ($D_{i1,+}$ is large to enclose the sphere of radius $D_{j2,+}$). This is analogous to Case 3.

702 the most common) we examine a random point in the spherical cap
 703 belonging to Sph.1 generated by the intersection of spheres Sph.1 and
 704 Sph.3 as illustrated in Fig. D.17(a). Once this point is selected, the
 705 position of monomer s1 is finally set by a displacement of the radius
 706 of monomer s1 (r_{s1}) in the unitary direction defined by CM1 and the
 707 current position of s1 (vector pointing to s1). Additionally, the spheres
 708 Sph.1 and Sph.4 can also intersect. In this case, the solution is found
 709 in the spherical segment illustrated in Fig. D.17(b).

710 Any point in the spherical cap (Fig. D.17(a)) or spherical segment
 711 (Fig. D.17(b)) can be a solution for finding a point contact between
 712 s1 and s2; however, this process of search may be very time consum-
 713 ing. That is the reason why FracVAL offers the option of enabling or
 714 disabling (by a binary value in the code) the search of random points
 715 on these surfaces. The other option is simply to select the intersection
 716 between the two larger spheres as described in section 3.2.

- 717 • Scenario 2: When $\Gamma_{12} < D_{s1,+} - D_{s2,+}$ and $\Gamma_{12} > D_{s1,-} - D_{s2,+}$. In this
 718 case, we search a random point in the spherical cap belonging to Sph.2
 719 generated by the intersection of Sph.2 and Sph.3. Once this point is
 720 selected the position of s1 is finally set by a displacement of r_{s1} in the
 721 unitary direction defined by CM1 and the current position of s1 (vector
 722 pointing to s1). Please refer to the illustration of Fig. D.18(a), as can

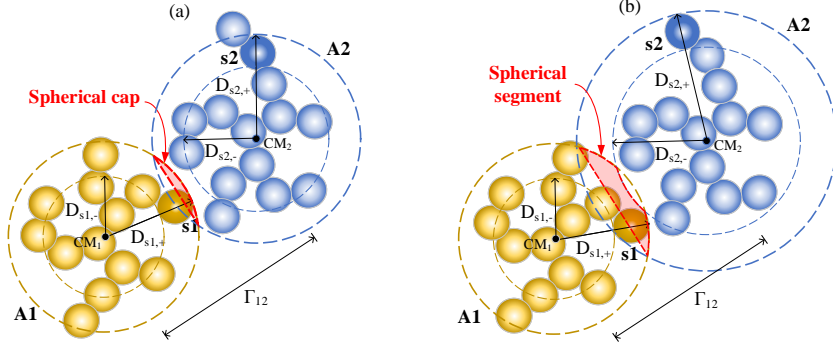


Figure D.17: (a) Spherical cap corresponding to A1, given by the intersection of Sph.1 and Sph.3. (b) Truncated spherical cap or spherical segment corresponding to A1, given by the intersection of Sph.1 and Sph.3 and limited by Sph.4.

723 be seen, the solution of Scenario 1 is not possible because sphere Sph.1
 724 (radius $D_{s1,+}$) is too big and therefore there is no intersection with
 725 sphere Sph.3 (radius $D_{s2,+}$). In this case, the position of monomer s1
 726 is found in the spherical cap of sphere Sph.2 (radius $D_{s1,-}$) generated
 727 by the intersection of spheres Sph.2 and Sph.3.

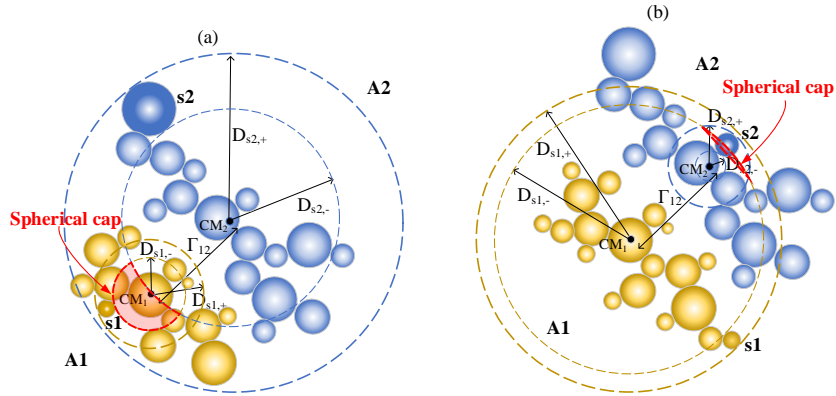


Figure D.18: (a) Example of scenario 2. (b) Example of scenario 3.

728 • Scenario 3: When $\Gamma_{12} < D_{s2,+} - D_{s1,+}$ and $\Gamma_{12} > D_{s2,-} - D_{s1,+}$. In
 729 this case, we examine a random point in the spherical cap belonging

730 to Sph.2 generated by the intersection of Sph.2 and Sph.4. Once this
731 point is selected the position of s1 is finally set by a displacement of
732 r_{s1} in the opposite unitary direction defined by CM1 and the current
733 position of s1 (vector pointing to s1). The solution of Scenario 1 is not
734 possible because sphere Sph.3 (of radius $D_{s2,+}$) is large and therefore
735 there is no intersection with sphere Sph.1 (of radius $D_{s1,+}$). In this
736 case, the position of monomer s1 is found in the spherical cap of sphere
737 Sph.2 (of radius $D_{s1,-}$) generated by the intersection of spheres Sph.2
738 and Sph.4 (please refer to Fig. D.18(b) for more details).